The Nitriding Behavior of Ti-Al Alloys at 1000 °C

J. MAGNAN, G.C. WEATHERLY, and M.-C. CHEYNET

The nitriding behavior of a series of alloys in the binary Ti-Al system has been determined at 1000 °C, under a controlled atmosphere of pure nitrogen gas, for times ranging between 7 and 100 hours. The scales and subscales were characterized by X-ray diffraction, scanning electron microscopy, transmission electron microscopy, energy dispersive and wavelength dispersive X-ray analysis, electron energy loss spectroscopy, and optical microscopy. Upon formation of a surface nitride scale, the subscale became enriched in Al and resulted in the formation of a series of Al-rich intermetallic phases. This enrichment has been linked to the transport processes in the scale and subscale and a shifting of the diffusion path toward the Al-rich corner of the ternary isotherm. The formation of Al-rich intermetallic phases in the subscale was shown to result in rapid ''breakaway'' nitriding of the TiAl and $TiAl_2$ alloys. The stoichiometry of the binary nitrides AlN and TiN was measured, as well as the composition of the ternary nitride ''Ti_2AlN.''

I. INTRODUCTION

TITANIUM aluminides have been developed for use in structural and aerospace applications where properties such as light weight and high strength, coupled with good high-temperature mechanical properties, are essential. One of the major concerns that must be resolved in order for these alloys to gain widespread use is their poor oxidation resistance.

At present, the maximum operating temperature of these aluminides is determined by the onset of rapid oxidation.[1,2] Previous studies have shown that the oxidation resistance of titanium aluminides is dependent on the oxidation environment, and that the presence of even low concentrations of nitrogen was responsible for a transition from parabolic kinetics to breakaway oxidation for TiAl alloys.[3] It is believed that this phenomenon is due to nitrogen pickup in the metal or nitride formation in the initial reaction products. Meier *et al.*[3] have shown that the presence of nitrogen increased the oxidation rate by forming a nitride layer at the scale-alloy interface, which prevents alumina from forming a continuous protective layer. The mechanism of this ''nitrogen effect'' was demonstrated by Rakowski *et al.*,[4] who found that nitrides consisting of Ti_2AlN and TiN formed at the scale-alloy interface and that their presence disrupted the continuity of the passivating alumina scale. These titanium-rich nitrides would be subsequently converted to oxides at a later stage in the oxidation, allowing the formation of an oxide morphology with continuous paths of TiO_2, permeable to oxygen and nitrogen.

The formation of the nitrides at the metal-scale interface was also explained by Roy *et al.*[5] They contended that the solubility of oxygen in titanium aluminides was orders of magnitude higher than that of nitrogen, so that the nitrogen concentration at the interface would reach a sufficient level to form TiN, while the oxygen would go into solution in the subscale. A thermodynamic analysis showed that titanium oxide was more stable than TiN, so the nitride would eventually be transformed to an oxide at a later time during the oxidation. The network of TiO_2 created by this process would prevent the formation of a passivating Al_2O_3 scale.

It has also been suggested that the presence of nitrogen caused the subscale to become brittle and was responsible for ''breakaway oxidation.''[6] Nitrides were observed in all of the alloys that were exposed to air, and it was proposed that the volume change associated with the formation of TiN caused internal stresses and cracking in the scale, which would allow oxygen to penetrate to the base alloy. Becker *et al.*[6] also attempted to determine the nitriding behavior of Ti-Al alloys by exposing them to a nitrogen atmosphere at high temperature. However, significant oxidation occurred because they were unable to remove all the oxygen from the nitrogen gas. This effect is due to the high affinity that Ti and Al have for oxygen. In spite of this, these authors reported that for the TiAl alloy subjected to extensive nitridation, the scale consisted of a heterogeneous mixture of various nitride phases, while Al-rich phases were formed in the subscale. It was proposed that the presence of Al-rich phases in the subscale was related to the formation of the titanium-rich nitrides in the scale.

The first published Ti-Al-N ternary phase diagram at 1000 °C for this system was that of Schuster and Bauer.[7] In addition to the binary phases, they reported the presence of the hexagonal phase Ti_2AlN, previously discovered by Jeitschko *et al.*,[8] as well as a new ternary nitride Ti_3AlN, having a perovskite structure. A subsequent study concluded that the isothermal section proposed by Schuster and Bauer had been obtained from samples that had not reached equilibrium.[9] Therefore, a new 900 °C ternary isotherm was proposed by Durlu *et al.*[9] to replace the previous 1000 °C isotherm of Schuster and Bauer.[7]

The nitrogen compositions of the ternary compounds have recently been measured using Dumas chromatography, assuming that the Ti/Al ratio was given by the structural formula, and were found to be nonstoichiometric.[10] The ternary perovskite structure compound was found to have a stoichiometry of $Ti_3AlN_{0.56}$. The more stable hexagonal phase had a measured stoichiometry of $Ti_2AlN_{0.82}$. The compositions of the binary nitrides have been more

J. MAGNAN, Graduate Student, and G.C. WEATHERLY, Professor, are with the Department of Materials Science and Engineering, McMaster University, Hamilton, ON, Canada L8S 4L7. M.-C. CHEYNET, Research Engineer, is with the Laboratoire de Thermodynamique et Phisico-Chimie Metallurgiques, INPGrenoble, 38402 Saint Martin d'Hêres, France.

Manuscript submitted February 20, 1998.

extensively studied and are shown in the respective binary phase diagrams.[11] No mutual solubility of AlN and TiN has been reported under equilibrium conditions, although high solubilities have been reported for (Ti,Al)N films deposited under kinetically limited conditions.[12] These films are assumed to be metastable.[13]

In this article, the results of a comprehensive study of the nitridation behavior at 1000 °C of a series of Ti-Al alloys are reported. The evolution of the diffusion path for each alloy has been determined and related to the transport processes through the scale and subscale. The sequence of phases found in both the scale and subscale is related to the diffusion path on the ternary isotherm. An analysis of the composition of the ternary phase Ti_2AlN and the binary phases TiN and AlN was completed and compared to the accepted ternary isotherm. The mechanism for the rapid nitridation observed for the TiAl intermetallic compound is discussed.

II. EXPERIMENTAL PROCEDURE

In order to investigate the diffusion path taken during the nitriding of TiAl alloys, gas/solid diffusion couples were used. The solid component consisted of bulk Ti-Al alloys, which were prepared using elemental Al pellets and titanium crystals, each with a purity of 99.999 pct. The pure metals were weighed to the desired composition and arc melted in an argon atmosphere in a water-cooled hearth. The alloy button was remelted several times to promote homogeneity and was then heat treated in argon at 1000 °C for 100 hours to complete the homogenization of the sample. Alloys were verified by X-ray diffraction to have the desired crystal structure, and optical microscopy confirmed that a large grain size was obtained, up to 2 mm. In addition, energy dispersive spectroscopy (EDS) and wavelength dispersive spectroscopy were performed on polished sections of the alloys to check the uniformity of the composition of the alloy. No other elements were present in the alloys, above the detectable limit with these techniques. Small particles of Al_2O_3 were detected in some samples, but these did not appear to affect the nitriding process.

A solid solution α-Ti alloy and the compounds Ti_3Al, TiAl, $TiAl_2$, and $TiAl_3$ were studied. Several alloys were prepared for compounds having a wide range of compositional stability. In addition, some two-phase alloys were prepared from the titanium-rich side of the Ti-Al phase diagram, in order to verify more accurately the diffusion path. The alloys were sectioned as flat specimens having an area of 1 cm^2 and a thickness of 0.5 cm, and polished to a 0.3-μm surface finish before beginning the experiments. The specimens were cleaned with acetone and alcohol prior to introduction into the nitriding furnace.

The nitriding reaction chamber consisted of a quartz tube set inside a tube furnace held at 1000 °C and supplied with ultra-high-purity nitrogen gas flowing at a rate of 25 sccm. The nitrogen was additionally purified in a gas train consisting of Ascarite to remove carbon dioxide and Drierite ($CaSO_4$) to remove moisture. Oxygen contamination was then removed by passing through a tube furnace packed with copper turnings at 350 °C before entering the nitriding furnace. Silicone O-rings and high vacuum grease were used to maintain an airtight system. Furthermore, the specimens were placed on a titanium nitride plate and zirconium metal turnings were positioned in the vicinity, to aid in the removal of residual oxygen. The nitriding times varied from 7 to 100 hours and the samples were removed after the furnace had cooled to room temperature.

X-ray diffraction was used to identify the phases present in the nitride films. A Nicolet X-ray diffractometer with Cu K_α radiation was used. The evolution of the phases in the nitride films was followed by comparing the spectra for alloys nitrided for different times.

Fractured and polished cross-sectional samples of the nitrided alloys were prepared for examination in the scanning electron microscope (SEM) and electron microprobe. The cross sections were cold mounted and polished to a 0.3-μm finish. Thin foil cross sections were also prepared for some nitrided alloys for examination by electron microscopy (transmission electron microscope/scanning transmission electron microscope (TEM/STEM). These cross sections were prepared by mechanical thinning to less than 100 μm, followed by ion milling at liquid nitrogen temperatures until electron transparent. After mechanical thinning, some foils were made electron transparent using a focused ion beam apparatus, which resulted in foils having large, uniformly thin areas spanning the scale and subscale regions. Some nitride films were scraped and crushed, then deposited on holey carbon grids for examination in the STEM. Diffraction analysis was performed on a PHILIPS* CM12 TEM, while EDS linescans and electron energy loss spectroscopy (EELS) analysis were done using both a JEOL** 2010F TEM/STEM and a VG HB5 STEM. The quantification procedure for the nitrogen concentration acquired using EELS will be explained in Section III.

*PHILIPS is a trademark of Philips Electronic Instruments Corp., Mahwah, NJ.

**JEOL is a trademark of Japan Electronics Optics Ltd., Tokyo.

Composition profiles were acquired using a Cameca SX50 microprobe analyzer using Al_2Cu, AlN, and $TiAl_3$ standards for calibration. The microprobe results were compared to SEM backscattered micrographs of the same regions so that compositions could be assigned to the various phases that appeared in the micrographs. Energy dispersive spectroscopy was used to identify the phases in the SEM micrographs.

III. RESULTS AND DISCUSSION

A. *Diffusion Paths and Transport Mechanisms*

The composition profile for each alloy was obtained through the use of a combination of several analysis techniques such as SEM, TEM, X-ray diffraction, electron microprobe analysis, EDS, and EELS. This information can then be plotted on a ternary isotherm, which is a convenient way to represent the diffusion path in a ternary system. Ternary isotherms have been used by other authors investigating the interdiffusion processes in Ti-AlN diffusion couples,[14] to show the diffusion path. However, these authors did not make use of the most recently published ternary isotherm by Durlu *et al.*[9]

In order to present the results of this study without repeating many of the same observations, data that demon-

Table I. Summary of Phase Sequence in Nitride Film and Subscale for Each Alloy, for the Initial, Intermediate, and Final Stages of Nitriding*

Alloy	**Sequence of Phases:** Changes as Nitriding Time is Increased (Time ⇒)		
α-Ti	TiN Ti_2N α-Ti		
α-Ti + Ti_3Al	TiN Ti_3AlN Ti_3Al α-Ti + Ti_3Al	TiN Ti_3AlN Ti_2AlN Ti_3Al α-Ti + Ti_3Al	Ti Ti_2AlN Ti_3Al α-Ti + Ti_3Al
TiAl	TiN Ti_2AlN TiAl	TiN Ti_2AlN $TiAl_2$ TiAl	TiN + AlN Ti_2AlN $TiAl_3$ $TiAl_2$ TiAl
$TiAl_2$	TiN Ti_2AlN $TiAl_3$ $TiAl_2$	TiN + AlN Ti_2AlN $TiAl_3$ $TiAl_2$	
$TiAl_3$	AlN Ti_2AlN $TiAl_3$		

*No further changes in the sequence are observed up to the maximum test time of 100 h.

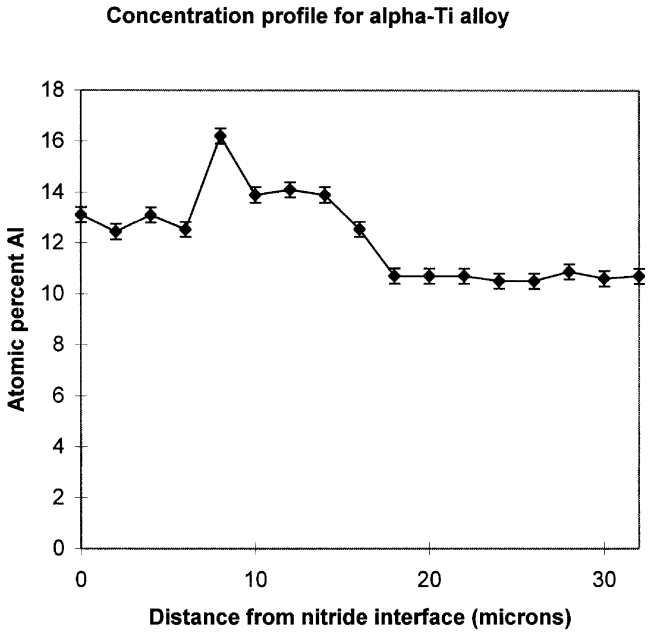

Fig. 1—Subscale concentration profile from an electron microprobe linescan, for a nitrided α-Ti alloy. The alloy becomes enriched in Al near the nitride interface and enters the two-phase region between α-Ti and Ti_3Al. The irregular concentration profile near the nitride interface is due to the presence of Al-rich Ti_3Al grains in the two-phase alloy region. The error bars are the standard deviation of the composition of the base alloy after nitriding.

strate the evolution of the diffusion path will be not be shown for all alloys. However, a summary of the sequence of phases present in the nitride layers and the subscale is shown in Table I, and the final diffusion paths for all alloys are superimposed on the ternary isotherm (Figure 18). Specific examples of alloys that best demonstrate the changing diffusion path will be explained in detail.

For all alloys, the diffusion path shifts away from the titanium corner, as is expected from the guidelines set out by Dalvi and Coates.[15] These authors have stated that the diffusion path will shift away from the most reactive component, which in this case is titanium since the free energy of formation at 1000 °C of TiN is more negative than the free energy of formation of AlN (−216 and −184 kJ/mol, respectively). This shifting of the diffusion path is a consequence of the change in composition of the subscale, as the surface nitride film is formed. The composition of the subscale changes because the nitrides formed on the surface of the alloy are titanium rich, and in order to satisfy the mass balance requirements, the excess Al diffuses into the subscale.

Aluminum-rich subscales were observed by Becker *et al.*[6] in nitrided regions of Ti-Al alloys exposed to various oxygen-nitrogen gas mixtures, but the mechanism for this enrichment was not fully explained. The results of the present study show that the Al enrichment in the subscale has important consequences on the sequence of phases formed in the scale and subscale. The nitrogen gas/Ti-Al alloy diffusion couple experiments are in agreement with the most recently published ternary phase diagram by Durlu *et al.*[9]

The nitriding behavior of each alloy will be discussed separately.

1. *α-Ti (11 atom pct Al) alloy*

This alloy demonstrated a behavior similar to that reported by Strafford and Towell[16] and is consistent with the phase diagram.[11] X-ray diffraction revealed that the scale consisted of TiN and η-Ti_2N. Significant enrichment of Al in the subscale was detected by electron microprobe profiles, from an initial composition of 11 to 14 at. pct Al at the interface between the Ti_2N and the α-Ti subscale after 100 hours of nitriding. It has been shown that the nitriding reaction is controlled by the supply of nitrogen atoms to the scale-metal interface.[16,17] As the titanium nitride scale grows, excess Al accumulates at the nitride-metal interface since the nitrides exhibit no significant Al solubility. In the present case, the subscale reached enrichment levels sufficient to enter the two-phase region between α-Ti and Ti_3Al, as demonstrated by the electron microprobe profile in Figure 1.

2. *Ti_3Al alloy*

Ti_3Al exhibited a planar and dense interface with the nitrides. A concentration gradient was present in the subscale, as for the α-Ti alloy (Figure 2). The shift in the concentration of the Ti_3Al alloy toward the Al-rich end of the phase diagram has significant consequences on the diffusion path, due to the location of the tie-lines between Ti_3Al and the Ti_3AlN and Ti_2AlN compounds. As shown on the equilibrium ternary phase diagram (Figure 5), the tie-lines run from Ti_3Al to Ti_3AlN at the titanium-rich side of the Ti_3Al stability field, while they run to the Ti_2AlN compound at the Al-rich end of the stability field. It is therefore possible that the subscale enrichment will result in an important change in the sequence of phases in the nitride scale. This study found that all alloys tested for 100 hours followed tie-lines to Ti_2AlN, even though their initial composition is adjacent to the tie-lines that run to the Ti_3AlN compound.

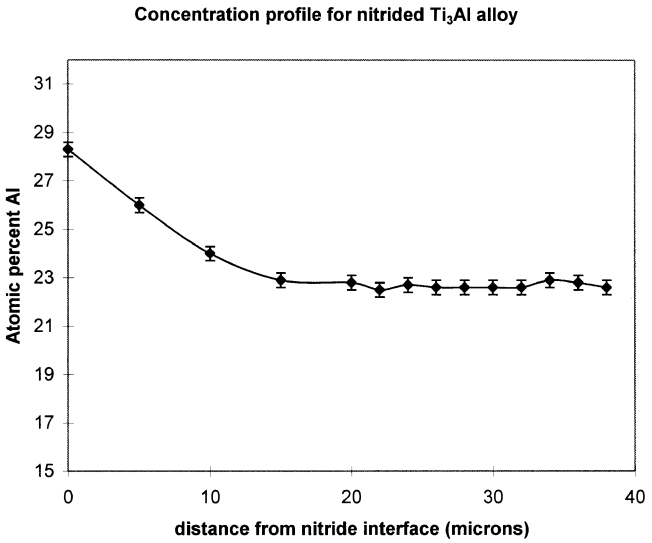

Fig. 2—Subscale concentration profile from an electron microprobe linescan, for a nitrided Ti_3Al alloy. Significant Al enrichment is present. The error bars are the standard deviation of the composition of the base alloy after nitriding.

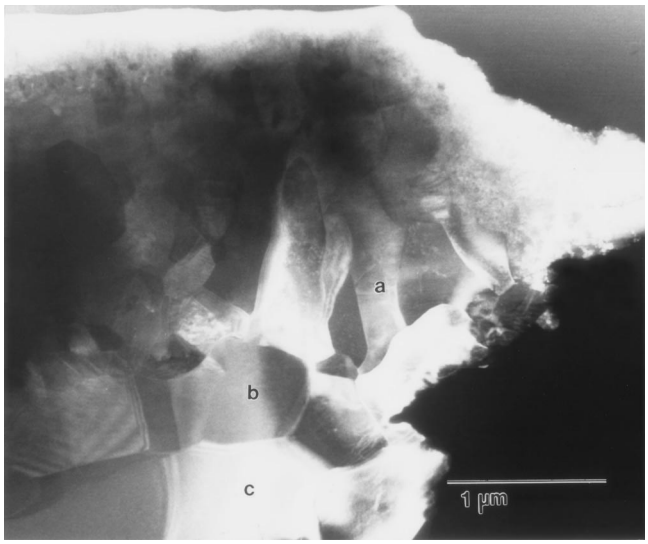

Fig. 3—STEM micrograph of a cross section of a nitrided Ti_3Al alloy. The various phases have been identified by electron diffraction. Region *a* = TiN, *b* = Ti_2AlN, and *c* = Ti_3Al.

This sequence of phases is shown in an STEM micrograph (Figure 3), where the various phases have been identified by electron diffraction.

In order to detect the Ti_3AlN phase, it was necessary to choose an initial alloy composition in the two-phase region between α-Ti and Ti_3Al. The path also shifted away from the titanium-rich side of the phase diagram, but for short times, the path entered the single-phase Ti_3Al stability field on the titanium-rich end of the phase diagram and then followed the tie-lines to the Ti_3AlN compound. If the alloy was nitrided for 100 hours, then the diffusion path would continue to shift until the alloy interface composition was in equilibrium with the Ti_2AlN ternary phase and consequently the Ti_3AlN phase disappeared. The presence of the Ti_3AlN phase could only be detected by X-ray diffraction, since the difference in the average atomic weight between

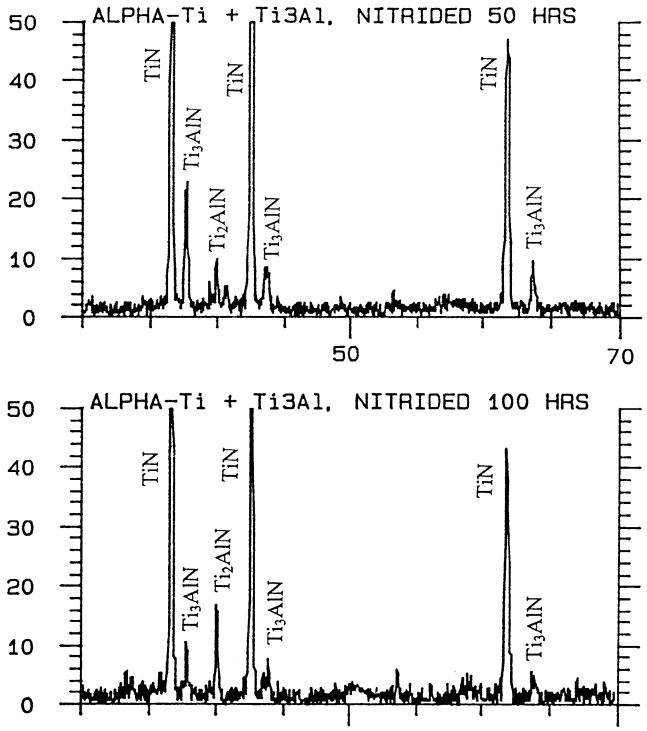

Fig. 4—X-ray diffraction spectra, showing the change in the phases present in the nitride scale of a nitrided α-Ti + Ti_3Al alloy, for times of 50 and 100 h. As the nitriding time is increased, the amount of the Ti_3AlN phase in the scale decreases, due to the shift in the diffusion path.

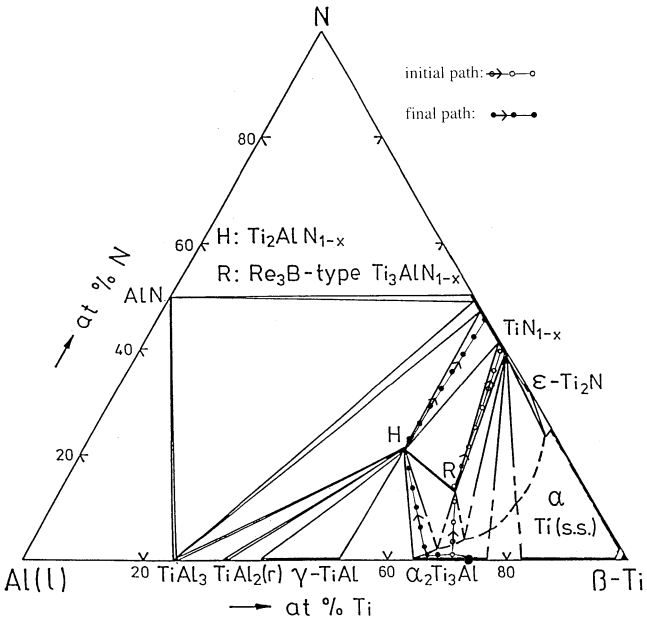

Fig. 5—Plot of the diffusion paths on the isothermal ternary phase diagram for the initial and final (100 h) stages of nitriding for the Ti_3Al alloy.

Ti_3Al and Ti_3AlN was insufficient to obtain phase contrast in backscattered SEM micrographs for visual identification. X-ray spectra for alloys tested for 50 and 100 hours are shown for comparison in Figure 4, which demonstrates that the Ti_3AlN phase is replaced by the Ti_2AlN phase as the nitriding time is increased. The shifting diffusion paths have been plotted on the ternary isotherm in Figure 5 in

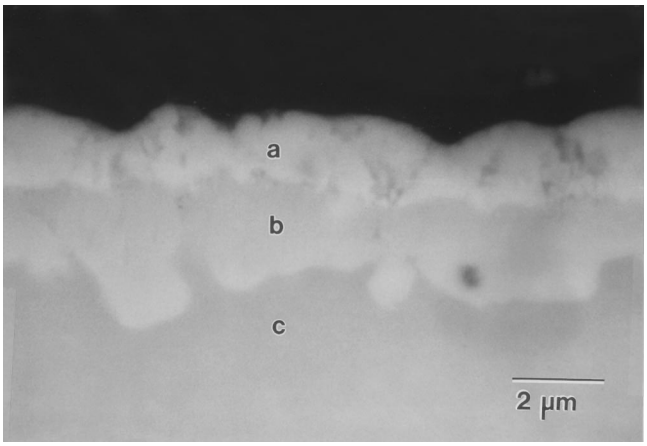

Fig. 6—SEM micrograph of cross section of TiAl alloy after 15 h of nitriding. Region a = TiN, b = Ti_2AlN, and c = TiAl.

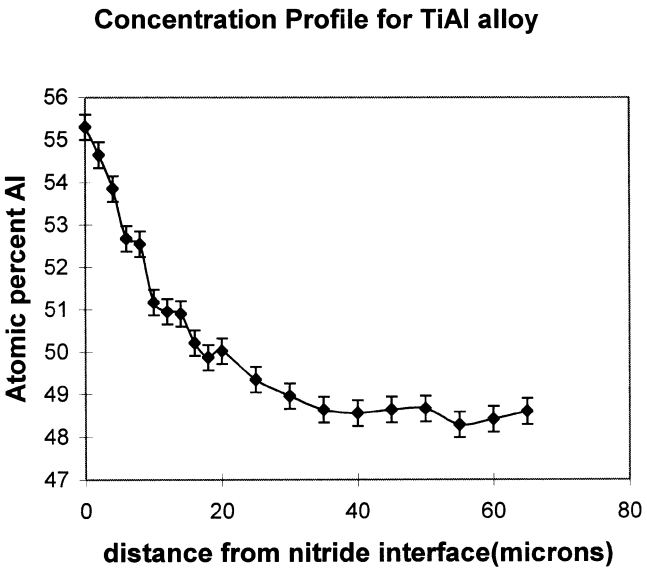

Fig. 7—Subscale concentration profile from electron microprobe linescan, for the alloy shown in Fig. 6. The TiAl subscale region is Al rich near the reaction interface. The error bars are the standard deviation of the composition of the base alloy after nitriding.

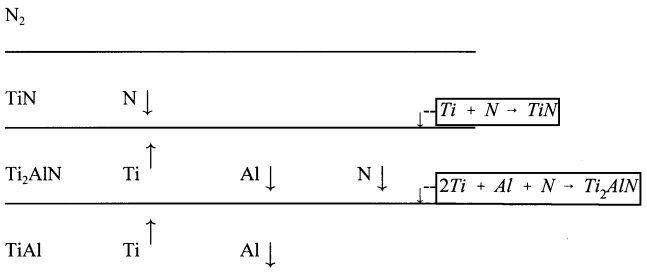

Fig. 8—Fluxes and interface reactions in the formation of nitrides on TiAl substrate.

order to illustrate the changes that occur during the enrichment of the subscale for Ti_3Al alloys.

3. *TiAl alloy*

The TiAl alloy exhibits the most complicated nitriding behavior of all the alloys, since many composition-induced phase transformations take place in the subscale as the nitriding reaction proceeds and Al enrichment continues below the nitride/subscale interface. The evolution of the diffusion path will be illustrated with electron microprobe linescans perpendicular to the reaction interface. These profiles will be compared to SEM and STEM micrographs of the same regions.

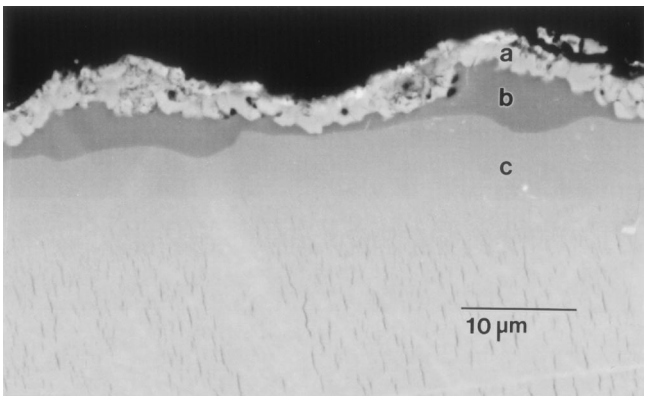

Fig. 9—SEM micrograph of cross section of TiAl alloy after 25 h of nitriding. Region a = TiN and Ti_2AlN, b = $TiAl_2$, and c = TiAl.

In the initial stages of nitriding, a nitride film consisting of an outer layer of TiN and an inner layer of Ti_2AlN forms at the surface of the TiAl alloy as determined by X-ray diffraction and EDS (Figure 6). Near the reaction interface, the alloy becomes enriched in Al as illustrated by the microprobe linescan (Figure 7). Since both nitride compounds have a higher Ti/Al ratio than TiAl, excess Al is rejected below the interface, enriching the TiAl subscale with Al. The level of enrichment of the subscale is high, so any outward diffusion of Al through the nitride layers must be minimal. The mechanism of enrichment is the same as for the Ti_3Al alloy, with nitrogen diffusing to the scale-metal interface and reacting with TiAl to form Ti_2AlN. The excess Al diffuses into the TiAl subscale, resulting in an enrichment in Al at the scale-metal interface. TiAl has a wide range of compositional stability at 1000 °C, from 48 to approximately 56 at. pct Al, so the TiAl phase can accommodate the Al enrichment up to 56 at. pct Al before becoming supersaturated. Significant Al enrichment is shown by the subscale concentration profile obtained by electron microprobe analysis (Figure 7). The flux of Ti, Al, and N and the reactions to form the TiN and Ti_2AlN phases are summarized in Figure 8. The diffusion path in the initial stages can be mapped on the ternary isotherm by moving from the initial alloy composition to a point of higher Al concentration in the TiAl phase field, then following the tie-lines, first to the Ti_2AlN compound and then to the TiN compound. This is shown in Figure 13.

When the subscale becomes sufficiently supersatured in Al, a new intermetallic compound, $TiAl_2$, is nucleated in order to accommodate the continued accumulation of Al. This step is necessary since the rate of removal of the excess Al by interdiffusion in the subscale is slower than the rate of production of excess Al by the nitriding reaction. The new sequence of phases is shown in Figure 9. The reduction in the supersaturation of the TiAl phase can be seen by superimposing the microprobe profiles before and after nucleation of $TiAl_2$. Figure 10 shows that the interfacial concentration of Al in TiAl before nucleation of

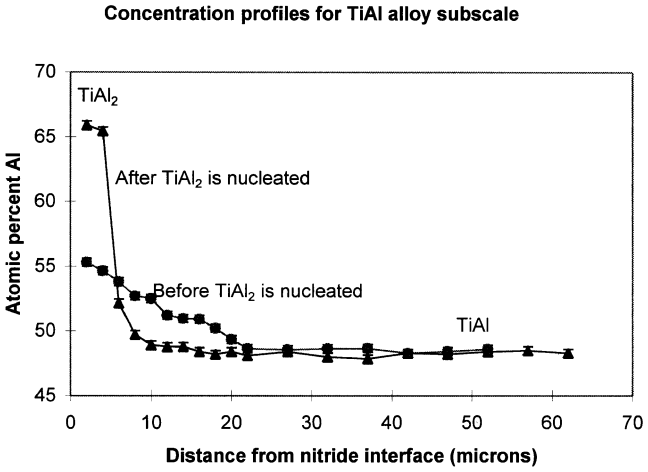

Fig. 10—Comparison of microprobe concentration profiles before and after nucleation of the $TiAl_2$ phase. The supersaturated Al in the TiAl phase is consumed and transformed to $TiAl_2$. The error bars are the standard deviation of the composition of the base alloy after nitriding.

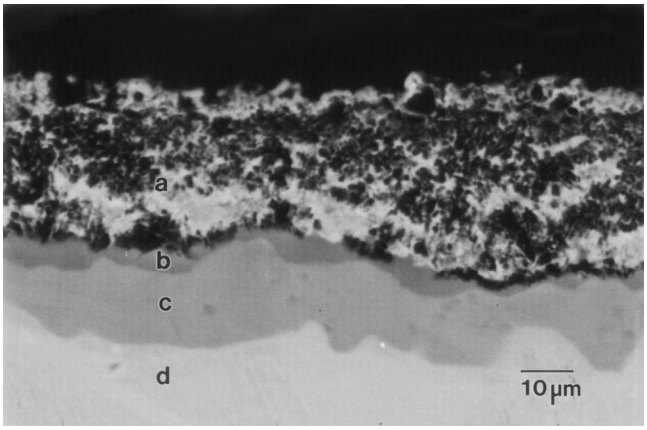

Fig. 11—SEM micrograph of cross section of TiAl alloy after 100 h of nitriding. Region a = mixed nitrides consisting of TiN, AlN and Ti_2AlN, b = $TiAl_3$, c = $TiAl_2$, and d = TiAl.

$TiAl_2$ is much higher than after nucleation of $TiAl_2$. It is no longer necessary for the TiAl phase to continue to absorb all the excess Al since the Al can be accommodated by the transformation.

$$TiAl + Al \rightarrow TiAl_2$$

The thickness of the $TiAl_2$ phase will continue to increase, as a means of accommodating the Al by-product produced during the nitriding reaction, since the $TiAl_2$ compound is almost stoichiometric. The formation of the $TiAl_2$ phase occurs more rapidly when the starting alloy composition is richer in Al, since less time is required to build up sufficient levels of Al at the interface to nucleate $TiAl_2$. The diffusion path for the second stage is also superimposed on the ternary isotherm in Figure 13.

After long times, a third change in the sequence of phases occurs, with the nucleation of a third intermetallic compound ($TiAl_3$) in the subscale, at the nitride/subscale interface. At the same time, the outer nitride scale becomes a heterogeneous mixture of Ti_2AlN, TiN, and AlN. This sequence of phases is shown in Figure 11.* The formation of the $TiAl_3$ intermetallic can again be explained in terms of the kinetics of diffusion of Al away from the reaction interface. In the intermediate stage, the growth of the $TiAl_2$ layer can be considered to be occurring under quasi-steady-state conditions:

$$J_{Al} \propto \frac{\delta \xi}{\delta t} = -D_{Al} \frac{C_1 - C_2}{\xi}$$

using the approximation that TiAl and $TiAl_2$ have the same molar volume. The term J_{Al} is the flux of Al atoms, ξ is the thickness of the $TiAl_2$ layer, C_1 is the concentration of Al in $TiAl_2$ at the nitride/$TiAl_2$ interface, C_2 is the concentration of Al in TiAl at the $TiAl_2$/TiAl interface, and D_{Al} is the interdiffusion coefficient of Al in $TiAl_2$. (Although N diffusion into the intermetallic layers might be occurring, the equilibrium solubility of N in TiAl is of the order of 40 ppm.[18] We were not able to detect N in any of the intermetallic phases by EELS analysis. Effectively all the N must be consumed at the nitride/alloy interface during the growth of the nitride scale.) The preceding equation shows that as ξ increases, the flux J_{Al} will decrease. Once the flux is no longer sufficient to remove the excess Al being produced at the nitride/subscale interface, the Al concentration will build up and supersaturate the $TiAl_2$ compound, which has a very limited range of compositional stability. At this point, the $TiAl_3$ phase will nucleate in order to accommodate the excess Al. Since both the $TiAl_2$ and $TiAl_3$ phases have a very limited compositional stability range and can be considered to be nearly stoichiometric, the excess Al will be consumed by following the reaction

$$TiAl_2 + Al \rightarrow TiAl_3$$

A significant change in the morphology and composition of the nitride scale accompanies the formation of the $TiAl_3$ intermetallic compound in the subscale. This change is demonstrated by the X-ray diffraction results before and after the final stage of nitriding (Figure 12). This is due to the change in the diffusion path and the mechanical breakdown of the scale. The mechanical breakdown of the scale may be linked to the presence of the brittle $TiAl_3$ compound in the subscale, since spalling is only present once the $TiAl_3$ intermetallic has formed. Rapid breakaway nitriding continues as the reaction time is increased and a heterogenous mixture of nitrides continues to form. No further changes in the sequence of phases was observed with increasing nitriding time.

Energy dispersive spectroscopy and EELS measurements performed on the outer scale material on the VG HB5 STEM indicated that only TiN and AlN were present, whereas Ti_2AlN, TiN, and AlN were identified in the areas of the nitride scale near the reaction interface. The heterogeneous nature of the nitride film and the nonplanar interface are an indication that tie-lines are being cut and/or a three-phase region on the ternary isotherm is entered. This

*In all the experiments, the thickness of the nitride layers (a few microns) is much less than the sample thickness (5, mm), so that the diffusion ''couple'' can be considered to be an infinite source of N_2 in contact with an infinite source of TiAl. Clearly, the global system cannot reach true equilibrium, but the attainment of local equilibrium at interface boundaries for experiments performed at 1000 °C and for durations up to 100 h seems plausible.

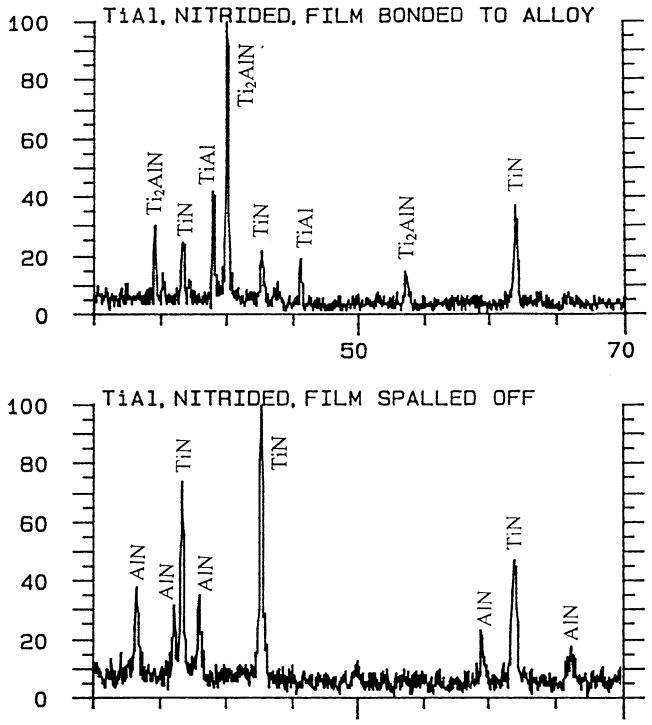

Fig. 12—X-ray diffraction spectra, showing the phases present in the nitride scale before and after spalling.

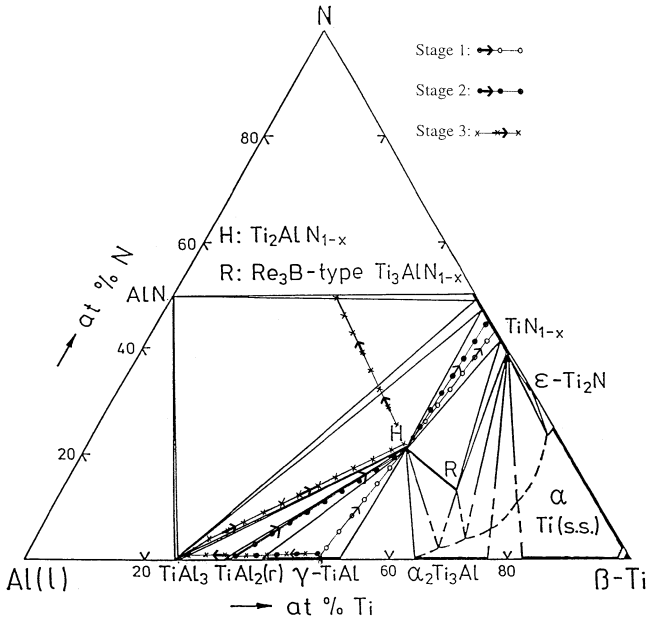

Fig. 13—Plot of the diffusion paths on the isothermal ternary phase diagram for first, second, and final stages of nitriding for the TiAl alloy.

final stage of nitriding has also been superimposed on the ternary isotherm in Figure 13.

Since the subscale continues to be enriched in Al after $TiAl_3$ is formed, liquid Al might form at the reaction interface. Thermodynamic calculations show that this step is never attained, since the free energy associated with the overall nitriding reaction,

$$2TiAl_{3(s)} + \frac{1}{2}N_{2(g)} \rightarrow Ti_2AlN_{(s)} + 5Al_{(l)}$$

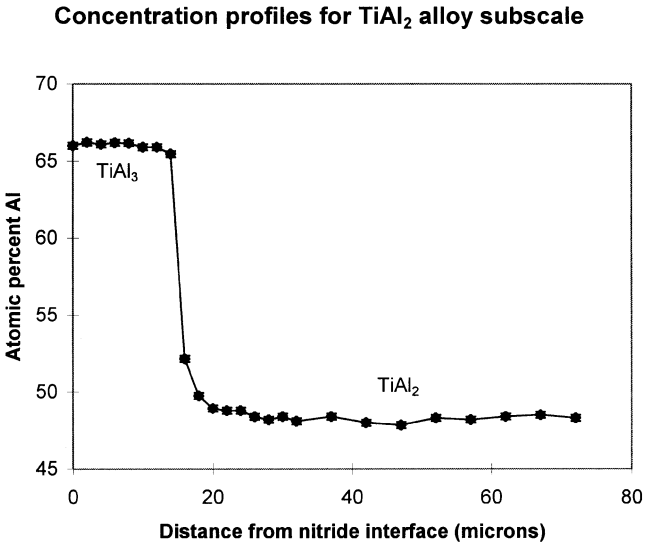

Fig. 14—Subscale concentration profile from an electron microprobe linescan, for a nitrided $TiAl_2$ alloy, shown in Fig. 14. In order to accommodate the excess Al due to the formation of titanium-rich nitrides in the scale, a $TiAl_3$ layer forms at the reaction interface. Both phases have a limited range of stoichiometry. The error bars are the standard deviation of the composition of the base alloy after nitriding.

has a free energy change of +10.3 kJ/mol of Ti_2AlN,[19,20,21] which makes this reaction thermodynamically unfavorable. No data exist for the free energy of N dissolved in TiN, so the overall global reaction has been written in terms of N_2 gas reacting with the substrate. If the excess Al is converted to AlN according to the reaction

$$2TiAl_{3(s)} + N_{2(g)} \rightarrow Ti_2AlN_{(s)} + 5AlN_{(s)}$$

then the free energy change for the overall reaction is very negative, at −1429 kJ/mol of Ti_2AlN. These free energy arguments explain the absence of liquid Al and the presence of a heterogeneous mixture of various nitride phases when the $TiAl_3$ compound is present.

4. *$TiAl_2$ alloy*

The interdiffusion processes that take place during nitriding of a $TiAl_2$ alloy are similar to those in the final stage of the nitriding of the TiAl alloy, with the exception that a much thicker layer of $TiAl_3$ is formed below the nitride layer. In contrast to the TiAl alloy, which can absorb much of the initial excess Al due to its wide range of compositional stability, $TiAl_2$ has a limited composition range and any excess Al would be used to form and increase the thickness of the $TiAl_3$ intermetallic. Thus, $TiAl_3$ is present even for short nitriding times and thickens as the nitriding continues. Nitrogen must diffuse through the TiN and Ti_2AlN phases and is consumed by reacting at the $Ti_2AlN/TiAl_3$ interface with $TiAl_3$ to form more Ti_2AlN according to the reaction

$$2TiAl_3 + 0.5N_2 = Ti_2AlN + 5Al$$

A typical electron microprobe profile across the subscale is shown in Figure 14. Initially, a continuous dense film of Ti_2AlN and TiN is present, suggesting that the diffusion path follows the tie-line from $TiAl_3$ to Ti_2AlN then to TiN, but after longer times, a heterogeneous mixture of Ti_2AlN, TiN, and AlN is formed, indicating that the path enters a

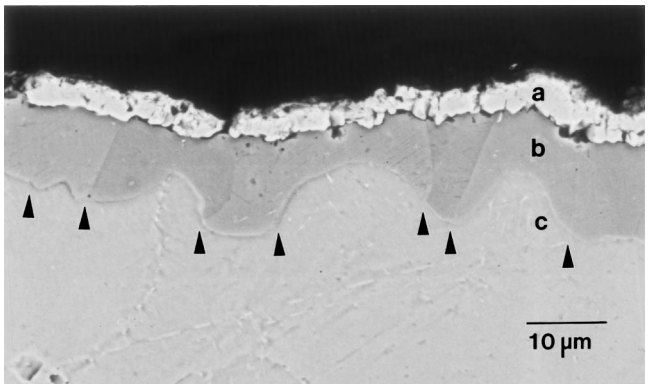

Fig. 15—SEM micrograph of a nitrided $TiAl_2$ alloy taken in backscattered mode, showing the $TiAl_3$ layer that forms in the subscale at the reaction interface in the initial stages of nitriding. Arrows mark the position of grain boundaries in the $TiAl_3$ phase. At these points, the growth of the $TiAl_3$ phase is fastest, due to rapid grain boundary diffusion. Region a = TiN and Ti_2AlN, b = $TiAl_3$, and c = $TiAl_2$.

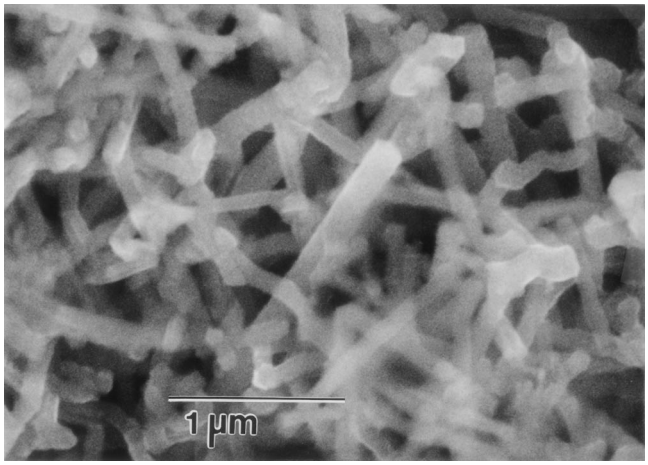

Fig. 16—SEM micrograph of the surface of a nitrided $TiAl_3$ alloy, showing high density of fine AlN needles. The composition of the needles is stoichiometric AlN.

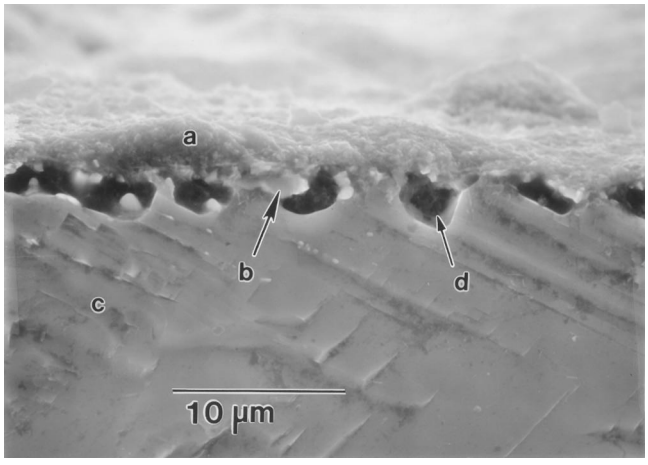

Fig. 17—SEM micrograph of a fracture surface cross section of a nitrided $TiAl_3$ alloy. Kirkendall porosity is visible at the nitride/$TiAl_3$ interface. Region a = AlN, b = Ti_2AlN, c = $TiAl_3$, and d = Kirkendall porosity.

three-phase region, as in the final nitriding stage of the TiAl alloy.

The subscale region presents another particular feature, easily identifiable due to the considerable thickness of the $TiAl_3$ layer. The interface between the $TiAl_2$ and $TiAl_3$ phases is very wavy. Closer investigation of this phenomenon revealed that this may be the result of significant grain boundary diffusion in the $TiAl_3$ phase. As the nitrides grow, the excess Al diffuses in the $TiAl_3$ phase away from the reaction interface and toward the $TiAl_2$ phase. This Al will preferentially diffuse along the grain boundaries, so that the $TiAl_3/TiAl_2$ interface will advance most rapidly at the grain boundaries. This effect is shown in Figure 15 for an alloy in the initial stages of nitriding. This evidence provides further support for the hypothesis that the excess Al from the nitriding reaction is transported to the subscale from the scale-metal interface where the nitriding reaction occurs.

5. *$TiAl_3$ alloy*

This alloy demonstrates the greatest resistance to nitriding, since only thin layers of nitrides are formed on its surface. The morphology of the scale presents two particular aspects, one being considerable porosity at the nitride/$TiAl_3$ interface and the other being the presence of a forest of AlN needles growing on the surface of the alloy (Figure 16). This morphology can be explained by considering the transport processes through a dense nitride layer, which consists only of Ti_2AlN. As the ternary nitride is formed, excess Al accumulates at the reaction interface. Since the alloy is stoichiometric, there is little possibility of absorbing more Al by inward diffusion. As shown earlier, the formation of liquid Al at the reaction interface is not thermodynamically feasible, so the Al diffuses outward, through the ternary nitride layer and forms AlN at the free surface. The outward movement of Al through the Ti_2AlN phase probably occurs by substitutional diffusion in the metal lattice, with a countercurrent flow of vacancies. These vacancies appear to accumulate and condense at the reaction interface, forming Kirkendall porosity. The SEM micrographs show that the porosity is faceted along certain crystallographic planes (Figure 17). Reports of Kirkendall porosity in the $TiAl_3$ compound can be found in the literature,[22] in support of this explanation. The different diffusion paths for Al in the $TiAl_3$ alloy and the $TiAl_2$ (and $TiAl_3$) alloy discussed earlier can be explained by considering how the excess Al produced during the conversion of $TiAl_3$ to Ti_2AlN is accommodated. When both $TiAl_2$ and $TiAl_3$ are present, Al can diffuse (along the $TiAl_3$ grain boundaries) away from the nitride interface, reacting with $TiAl_2$ to form $TiAl_3$ at the $TiAl_2/TiAl_3$ interface. On the other hand, if only $TiAl_3$ is present, the excess Al cannot diffuse toward the interior, since $TiAl_3$ is stoichiometric, and there is no $TiAl_2$ to consume the Al by forming $TiAl_3$. The only other path that can be taken by the excess Al is to diffuse outward through the $TiAl_2N$ phase in order to reach the outer surface, where it is converted to AlN. The diffusion of Al through Ti_2AlN is very slow,[23] which may explain the slow kinetics of nitridation of $TiAl_3$, as compared to the other binary Ti-Al alloys considered in this study.

The observed growth of fine AlN needles at the surface can be compared to similar morphologies observed during the oxidation of metals. Kofstad[24] has reported that whisker growth is sometimes observed during oxidation of Nb, Cu, and Fe. Several mechanisms describing the growth of these whiskers have been proposed, including short cir-

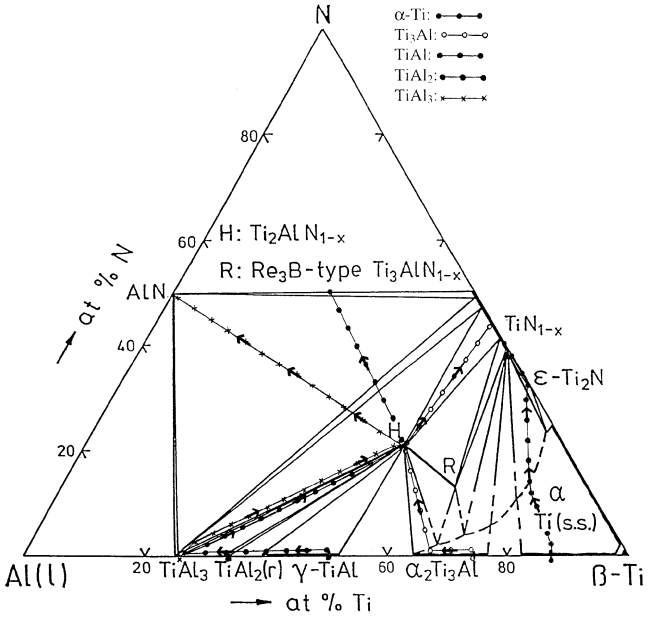

Fig. 18—Plot of the final diffusion paths on the isothermal ternary phase diagram for all the diffusion couples in this study.

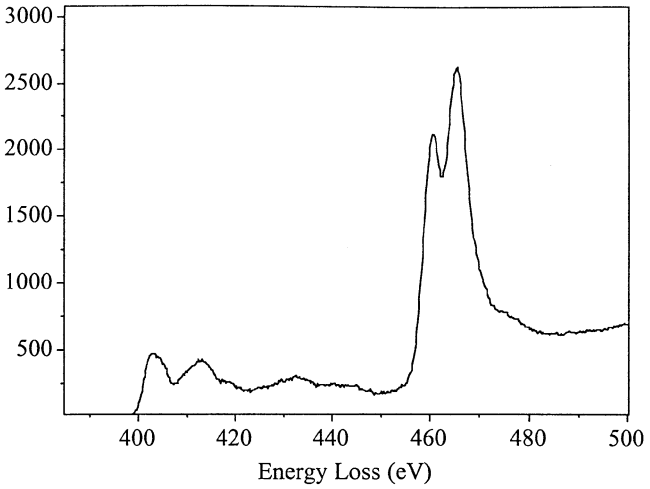

Fig. 19—EELS spectrum for the TiN phase, showing energy loss near edge structure at the nitrogen edge.

cuit diffusion up the center of the whisker blade, or an evaporation-condensation mechanism. In the present case, the growth of the whisker could take place at the root or the tip of the blade. The EELS analysis shows that the whiskers are stoichiometric AlN.

B. *Summary of the Diffusion Paths*

The final diffusion paths for all the alloys have been plotted on the ternary isotherm in Figure 18. For Ti_3Al alloys, the diffusion path shifts away from the tie-lines that lead to the Ti_3AlN compound and instead follow the tie-lines to the Ti_2AlN compound. For the TiAl and $TiAl_2$ alloys, the path shifts to the $TiAl_3$ compound, then goes to the Ti_2AlN compound before entering the three-phase region of Ti_2AlN, TiN, and AlN. The film is a heterogeneous mixture of nitrides and the interface becomes nonplanar. For the $TiAl_3$ alloy, the path follows the tie-line to the Ti_2AlN compound then heads to the AlN compound. Table I shows the evolution of the sequence of phases for all the alloys.

C. *Analysis of the Composition of the Nitrides*

In order to determine the composition of the ternary nitride Ti_2AlN and the binary nitride TiN, both EDS and EELS were used. The measurements were done independently on two different microscopes, using different acquisition conditions and analysis techniques. The procedure followed for the quantification of the nitrogen concentration results acquired on the VG HB5 by EELS was the standard technique explained by Egerton[25] with the EL/P software package. For the EELS results acquired on the JEOL 2010F, comparison to true standards was used in conjunction with the EL/P program. Two different TiN powder standards were prepared. The first was from a certified chemically analyzed (stoichiometric) powder obtained from Cerac Inc., Milwaukee, Wisconsin, while the second was obtained by arc melting the same powder under pure nitrogen. This second method sublimed the TiN and yielded an extremely fine powder, typically 10 to 20 nm in diameter. This was ideal for EELS analysis, since the particles had a thickness of only 0.2 to 0.3 λ, where λ is the mean free path. After background subtraction and removal of plural scattering effects, the area under the nitrogen K edge, located at 401 eV, was integrated over an energy window of 54 eV. This area was normalized by the height of the titanium L edge, located at 456 eV, in order to be able to compare different spectra. The experimental error inherent to this method is that the height of the titanium L edge depends on the level of background from the nitrogen K edge. However, the Ti-L peak is often an order of magnitude or more higher than this background level (Figure 19), and a check of the maximum possible error yielded a value of only 1 pct, which is less than the experimental scatter of the standards. The normalized results from 20 spectra from the two standards were averaged and found to have a standard deviation of 5 pct. This average was then considered to correspond to a 1:1 ratio of N:Ti. All other spectra were analyzed in the same manner, and the normalized area under the nitrogen K edge was compared to the value obtained for the standards.

The TEM foil used in the JEOL 2010F was prepared by the FIB technique, described in the experimental methods. Over 20 points were analyzed for the EDS measurements, while 10 points for EELS analysis were used to calculate the average composition. It appeared that beam damage was occurring when using a focused 0.5-nm-diameter probe for EELS analysis, since the N/Ti results were far lower and showed greater scatter than expected. Beam damage was minimized by acquiring the spectra using a scanned area of size 0.5 μm^2. The results of the Ti/Al ratio showed a very small standard deviation from point to point. The EELS results for the N/Ti ratio showed a greater variation, but the average was close to the value of the stoichiometric formula for Ti_2AlN and showed a small nitrogen deficiency in the TiN phase. The results are summarized in Table II.

The measurements made on the VG HB5 were acquired from nitride particles scraped from the surface of a nitrided alloy and placed on a holey carbon film supported by a copper grid. Since this sample contained TiN, Ti_2AlN, and

Table II. Summary of Compositions Measured with the JEOL 2010F

Compound	Ti/Al (EDS)	At. Pct Al in Metal Lattice	N/Ti (EELS)
Ti_2AlN	2.13 ± 0.02	31.9 ± 0.6	0.54 ± 0.07
TiN	—	2.0 ± 0.4	0.80 ± 0.12

Table III. Summary of the Compositions Measured on the VG HB5

Compound	Ti/Al (EDS)	At. Pct Al in Metal Lattice	N/Ti (EELS)	N/Al (EELS)
Ti_2AlN	2.12 ± 0.2	31.9 ± 6	0.53 ± 0.08	—
TiN	—	0 to 2.0	0.88 ± 0.11	—
AlN	—	100	—	0.98 ± 0.07

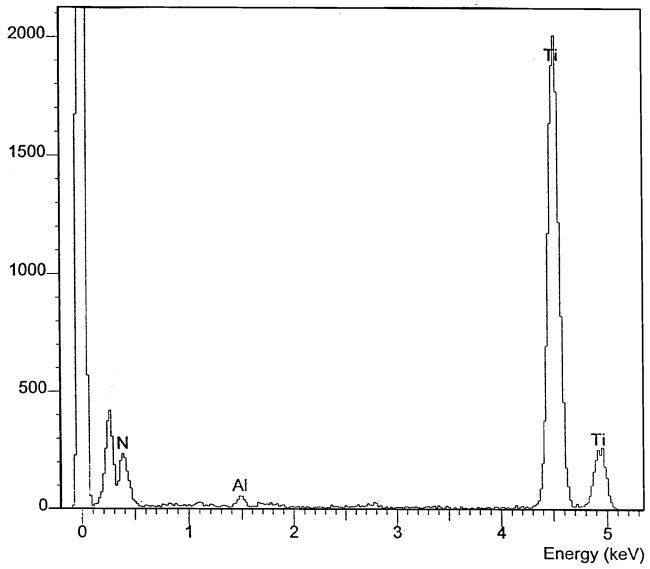

Fig. 20—EDS spectra from the TiN phase when the nitride film is well adhered to the TiAl alloy. The acquisition was done in STEM mode on a cross-sectional foil.

AlN particles, particle overlap might lead to spectra that were a combination of two or three phases. To avoid this problem, only those particles having a Ti fraction, as determined by EDS to be within 1 pct of the value calculated previously, were used to calculate the EDS and EELS average values for the Ti_2AlN compound. Similarly, only particles that yielded negligible Al contents were used for calculating the N/Ti ratio of the TiN compound. The N/Al ratio for AlN was determined from particles having a negligible Ti content. The EDS and EELS spectra were recorded simultaneously for the same point. The results are summarized in Table III.

Although the acquisition conditions and the operating conditions for the two microscopes were not the same, the results for the two instruments agree quite well, lending confidence that the reported values are close to the true value for the composition of these phases. Knowing the Ti/Al and N/Ti ratios, the stoichiometry of the so-called Ti_2AlN compound is found to be $Ti_{2.04}Al_{0.96}N_{1.09}$. Similarly,

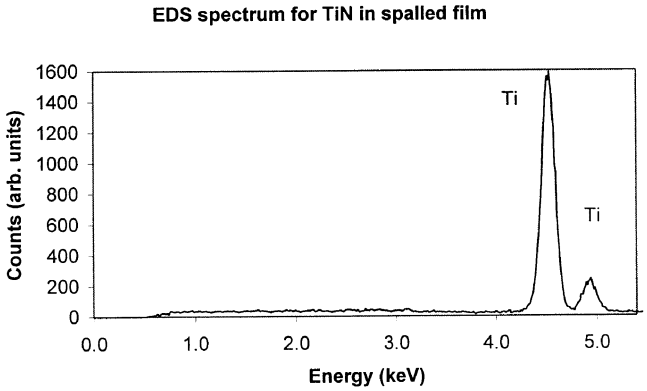

Fig. 21—EDS spectra from the TiN phase when the nitride film has spalled away from the subscale alloy. The acquisition was done in STEM mode on small particles on a holey carbon grid. No Al is present. The spectrum is cut off at approximately 600 eV because the detector is equipped with a beryllium window.

the stoichiometry of the titanium nitride phase, containing Al, is calculated to be $(Ti_{0.98}Al_{0.02})N_{0.84}$.

In specimens where the TiN phase adhered well to the Ti_2AlN phase, the TiN phase contained significant quantities of Al, so verification was done to ensure that this EDS measurement was not due to spurious X-rays originating from other parts of the specimen. TiN particles originating from the same sample from which the cross-sectional TEM foil was made were collected on a carbon film supported by a copper grid. Approximately 50 EDS acquisitions were performed on these particles, and none were found to contain less than 1.8 at. pct Al. Only a very low number of counts for Ti and Al X-rays were obtained when the beam was not focused on a particle, confirming that the Al signal in fact originated from the titanium nitride particles. Based upon the measurements of the particles and of the cross-sectional foil, the Al content in the TiN phase is 2.0 ± 0.4 at. pct.

Previous studies have not reported the presence of any Al in TiN, except in metastable films, sputter deposited at high deposition rates and low temperatures.[12,13,26] The specimens in which Al was detected in the TiN phase corresponded to conditions where the TiN phase adhered well to the Ti_2AlN phase. Other measurements on crushed powders of spalled scales from specimens nitrided for 100 hours, which contained no Ti_2AlN, revealed only pure TiN and AlN, with no mutual solubility (Figures 20 and 21). It appears that the high levels of Al in the TiN phase are related to the presence of the Ti_2AlN phase, and full phase separation occurs after the longest nitriding times, when the nitride scale consists of a heterogeneous mixture of nitrides.

Thermodynamic data describing the free energy of (Ti, Al)N films have been provided by Zeng and Schmid-Fetzer,[27] but vary considerably depending on the method used to fit all the thermodynamic parameters to the existing data. Significant difficulties were encountered by Zeng and Schmid - Fetzer when attempting to make all their data self-consistent. For this reason, it is not possible to determine whether the measured Al solubility in TiN is associated with a metastable state or is due to a stable equilibrium between TiN and Ti_2AlN. If the free energy surface of the (Ti, Al)N phase has a strong curvature near the Ti-rich boundary, a tangent plane to both the Ti_2AlN and TiN free

energy surfaces could contact the TiN surface at a point a short distance away from pure TiN. Since the tangent plane construction determines the equilibrium concentrations of the phases, this would describe an equilibrium solubility of Al in TiN. However, the lack of reliable thermodynamic data makes this determination inconclusive and the measured solubility of Al in TiN may reflect a metastable rather than a true equilibrium state.

IV. CONCLUSIONS

1. The diffusion processes that occur during nitriding of Ti-Al alloys at 1000 °C have been identified. The diffusion paths have been mapped out for each intermetallic compound in the Ti-Al system for exposure to nitrogen gas at 1000 °C. The diffusion paths shift toward the Al rich corner of the Ti-Al-N ternary isotherm in the subscale region and the overall behavior is manifested by Al enrichment in the subscale region. For the alloys TiAl and $TiAl_2$, this results in the formation of additional Al-rich intermetallics in the subscale. For the titanium rich alloy Ti_3Al, the shift in the diffusion path resulted in the disappearance of the Ti_3AlN phase at longer nitriding times, although this nitride phase is expected to be in equilibrium with Ti_3Al if the diffusion path did not shift.
2. For the TiAl alloy, spalling and rapid breakaway nitriding occurred once both $TiAl_2$ and $TiAl_3$ were formed in the subscale.
3. The diffusion paths observed for the Ti-Al alloy/N_2 diffusion couples were in agreement with the most recently published experimental phase diagram by Durlu *et al.*[9]
4. Kirkendall porosity was observed for the $TiAl_3$ alloy as a result of the different rates of diffusion of Ti and Al in this intermetallic compound.
5. The composition of the binary and ternary nitrides were carefully determined using EELS and EDS. The composition was $(Ti_{0.98}Al_{0.02})N_{0.84}$ for the TiN phase when in contact with the ternary nitride, but no solubility of Al was found when the nitride was not in contact with the substrate. The ternary nitride had a measured composition of $Ti_{2.04}Al_{0.96}N_{1.09}$.

ACKNOWLEDGMENTS

The authors are grateful to the National Sciences and Engineering Research Council (NSERC) of Canada and to the Ontario Centre for Materials Research (OCMR) for their support of this work.

REFERENCES

1. R. Beye, M. Verwerft, J.T.M. De Hosson, and R. Gronsky: *Acta Mater.*, 1996, vol. 44 (10), pp. 4225-31.
2. M. Dimiduk, B. Miracle, Y.-W. Kim, and M.G. Mendiratta: *Iron Steel Inst. Jpn. Int.*, 1991, vol. 31 (10), pp. 1223-24.
3. G.H. Meier, F.S. Pettit, and S. Hu: *J. Phys. IV*, Coll. C9, suppl. *J. Phys. III*, 1993, vol. 3, pp. 395-402.
4. J.M. Rakowski, F.S. Pettit, G.H. Meier, F. Dettenwanger, E. Schumann, and M. Ruhle: *Scripta Metall. Mater.*, 1995, vol. 33 (6), pp. 997-1003.
5. T.K. Roy, R. Balasubramaniam, and A. Ghosh: *Metall. Mater. Trans. A*, 1996, vol. 27A, pp. 4003-10.
6. S. Becker, A. Rahmel, M. Schorr, and M. Schutze: *Oxid. Met.*, 1992, vol. 38 (5–6), pp. 425-64.
7. J.C. Schuster and J. Bauer: *J. Solid State Chem.*, 1984, vol. 53, pp. 260-65.
8. W. Jeitschko, H. Nowotny, and F. Benesovsky: *Monatsh. Chem.*, 1963, vol. 94, pp. 1198-1200.
9. N. Durlu, U. Gruber, M.A. Pietzka, H. Schmidt, and J.C. Schuster: *Z. Metallkd.*, 1997, vol. 88 (5), pp. 390-400.
10. M. Pietzka and J.C. Schuster: *J. Am. Ceramic Soc.*, 1996, vol. 79 (9), pp. 2321-30.
11. T.B. Massalaski: *Binary Alloy Phase Diagrams*, ASM INTERNATIONAL, Metals Park, OH, 1990.
12. T. Wahlstrom, L. Hultman, J.-E. Sundgren, F. Adibi, I. Petrov, and J.E. Greene: *Thin Solid Films*, 1993, vol. 235, pp. 62-70.
13. H.A. Jehn, S. Hofmann, V.-E. Ruckborn and W.-D. Munz: *Journal of Vacuum Science Technol. A*, 1986, vol. 4 (6), pp. 2701-12.
14. M.H. El-Sayed, M. Naka, and J.C. Schuster: *J. Mater. Sci.*, 1997, vol. 32, pp. 2715-12.
15. A.D. Dalvi and D.E. Coates: *Oxid. Met.*, 1972, vol. 5 (2), pp. 113-35.
16. K.N. Strafford and J.M. Towell: *Oxid. Met.*, 1976, vol. 10 (1), pp. 41-67.
17. F. Anglezio-Abautret, B. Pellissier, M. Miloche, and P. Eveno: *J. Eur. Ceramic Soc.*, 1991, vol. 8, pp. 299-304.
18. M.J. Kaufmann, D.G. Karitzer, R.D. Shull, and H.L. Fraser: *Scripta Metall.*, 1986, vol. 20, pp. 103-08
19. R. Schmid-Fetzer and K. Zeng: *Metall. Mater. Trans. A*, 1997, vol. 28A, pp. 1949-51.
20. A.T. Dinsdale: *Data for Pure Elements*, Scientific Group Thermodata Europe (SGTE), *CALPHAD*, 1991, vol. 15 (4), pp. 317-425.
21. N. Dupin: Ph.D. Thesis, Institut National Polytechnique de Grenoble, Grenoble, France, 1995.
22. E.P. George, J.A. Horton, W.D. Porter, and J.H. Schneibel: *J. Mater. Res.*, 1990, vol. 5 (8), pp. 1639-48.
23. S. Becker, A. Rahmel, M. Schorr, and M. Schutze: *Oxid. Met.*, 1992, vol. 38, pp. 425-64.
24. P. Kofstad: *High Temperature Corrosion*, Elsevier Applied Science Publishers Ltd., New York, NY, 1988.
25. R.F. Egerton: *Electron Energy Loss Spectroscopy in the Electron Microscope*, 2nd ed., Plenum Press, New York, NY, 1996.
26. T. Ikeda and H. Satoh: *J. Jpn. Inst. Met.*, 1993, vol. 57 (8), pp. 919-25.
27. K. Zeng and R. Schmid-Fetzer: *Thermodynamic modeling and applications of the Ti-Al-N Phase Diagram, Thermodynamics of Alloy Formation*, Y.A. Chang and F. Sommer, eds., TMS, Warrendale, PA, 1997, pp. 275-94.